Dynamic Road Surface Signatures in Automotive Scenarios

Bouwmeester, Wietse; Fioranelli, Francesco ; Yarovoy, Alexander

DOI
10.23919/EuRAD50154.2022.9784570

Publication date
2022

Document Version
Final published version

Published in
Proceedings of the 18th European Radar Conference

Dynamic Road Surface Signatures in Automotive Scenarios

Wietse Bouwmeester, Francesco Fioranelli, Alexander Yarovoy

MS3 Group, Department of Microelectronics, Delft University of Technology, The Netherlands

{w.bouwmeester, f.fioranelli, a.yarovoy}@tudelft.nl

***Abstract* — A method to compute road surface signatures in the automotive scenario is presented. This method is subsequently applied to a rough asphalt surface without undulations. It is shown that, due to the observation geometry, the road surface signature experiences significant spreading along the Doppler-axis, resulting in a distinct range-Doppler map that could be used for classification purposes. This was also confirmed with an experimental recording from a car driving around the university campus. The variation of Doppler-shift and incident angle within a range bin and over a coherent processing interval is also evaluated.**

***Keywords* — Autonomous vehicles, Advanced driver assistance, Radar cross-sections, Rough surfaces scattering**

I. Introduction

Throughout the years, several frequency bands have been made available for automotive radar purposes, starting with the 24 GHz band and nowadays the main 77-81 GHz band. At these higher frequencies, more bandwidth is available, which results in better range resolution [1]. Furthermore, the scattering behaviour of targets is different at higher frequencies. For instance, a road surface may act as a flat smooth surface at 24 GHz, while it could appear rough at 79 GHz, which increases detectability by radar as stronger backscattering occurs.

The ability to measure backscattering from road surfaces provides an unique opportunity to enhance the performance of road safety systems such as anti-lock breaking. Namely, if these systems could be provided with an estimation of the road surface conditions up ahead, they can already be set to expect a specific surface friction coefficient and therefore find more quickly their optimal control inputs. This could result in a quicker emergency stop. For autonomous driving, potential hazards such as patches of ice could even be avoided altogether by exploiting the different backscattering properties of road surfaces for automatic classification purposes.

In this paper, a method is presented to compute the signature of road surfaces, which can be exploited in future research to automatically identify dangerous surfaces (e.g. patches of water and ice) ahead of the vehicle. This method considers road surface scattering from the radar's point of view and takes the dynamics of the automotive scenario into account. This fills the gap in literature for road surface scattering in dynamic scenarios as previous research has mainly focused on road surface scattering in the static case [2], [3]. Besides this, other research in the area of road surface classification has been measurement-focused ([4], [5]), whereas the method developed here may be used for a more analytical approach to road surface classification, and thereby gain more physical insight in this challenging scattering problem. The presented method is also able to take undulations in the road surface in account.

The rest of the paper is organised as follows. Section II treats the effects of the radar observation geometry on the road surface scattering. Section III explores the geometrical effects when applied to a rough road surface without undulations. Section IV presents a range-Doppler map of the signature of an asphalt road surface and section V concludes the paper.

II. Influence of Geometrical Effects on Road Surface Signatures

In the automotive radar scenario, two important factors that influence scattering from road surfaces need to be considered. Firstly, the angle of incidence varies from range cell to range cell as well as with azimuth. Secondly, when the car is moving, a Doppler-shift will be induced depending on the radial velocity corresponding to the range-azimuth cell the radar is observing.

The first effect influences the amount of scattering that will happen within a range cell. To illustrate, when the angle of incidence is close to the horizon, generally less radiation is scattered back from a rough surface than from an incident angle close to the normal. The second effect will cause the signature of the road surface to spread along the Doppler axis of the range-Doppler map, i.e. a cell that is right in front of the car will have a higher radial velocity and thus a larger Doppler-shift than a cell orthogonal to the direction of travel.

In FMCW radar systems using multiple pulses per frame, the amount of range migration, variation in incident angle and Doppler-shift of a surface patch over the coherent processing interval must be considered. If this variation is significant, the observed scattering may be affected and more sophisticated electromagnetic techniques need to be developed to account for such variations. Equally, the variation of incident angle and Doppler-shift within one range cell must be considered. Lastly, the signature of the road surface is also influenced by the radiation pattern of the radar system. If the gain changes significantly from pulse to pulse within a range bin, this effect needs to be taken into account as well.

Here, a method is presented to evaluate the severity of the mentioned effects for a specified road surface. First

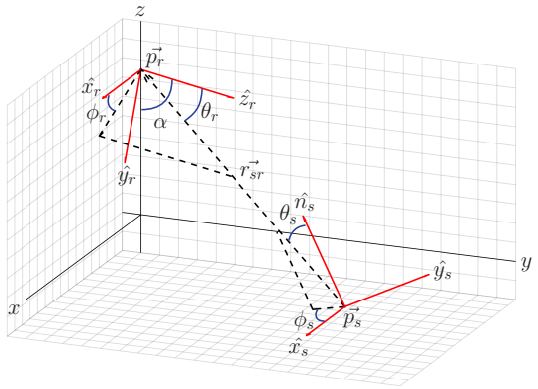

Fig. 1. Geometrical parameters used for computing surface scattering.

the definitions of geometrical parameters will be presented. Afterwards, the derivation of incident angle, radial velocity and local radar observation angle will be shown. The last mentioned quantity is required to calculate the radar antenna gain for that surface point.

A. Geometrical Parameter Definitions

The radar location is indicated by the vector $\vec{p_r} = \{0, 0, h_r\}$. Here, h_r indicates the height of the radar above ground level. The position of a point on the surface is indicated by the vector $\vec{p_s} = \{x_s, y_s, z_s\}$. Each surface point is also characterised by a normal vector, which is defined as $\hat{n_s} = \{x_{\hat{n}}, y_{\hat{n}}, z_{\hat{n}}\}$. The set of angles of incidence at a surface point are designated as θ_s and ϕ_s. Here, θ_s is the angle between the surface normal, representing the surface local z-axis, and the vector $\vec{r_{sr}}$, which is the vector pointing from the surface point to the radar. The surface local x-axis is defined in such a way that it lies on the global xz-plane. This surface local x-axis is used to compute the azimuth angle of the incident wave ϕ_s.

The radar local observation angles are defined by θ_r and ϕ_r. Here, the elevation θ_r is measured from the radar broadside direction, indicated by the z-axis in the radar local system. Likewise, ϕ_r is the azimuth measured from the x-axis in the radar local system. The angle between the radar local z-axis and the global x, y-plane is designated by the angle α.

Lastly, the velocity of the car is indicated by the vector $\hat{v_c} = \{0, v_c, 0\}$. Note from this vector that the car is travelling along the $\hat{y}$ direction. A summary of these geometrical parameters is shown in Fig. 1.

B. Derivation of Parameter Expressions

The angle θ_s can be found in a two-step process. The first step is to find the vector from the surface point to the radar location which can be calculated using $\vec{r_{sr}} = \vec{p_r} - \vec{p_s}$. Subsequently, the surface local θ_s can be found using (1).

$$\theta_s = \cos^{-1}\left(\frac{\vec{r_{sr}} \cdot \hat{n}_s}{|\vec{r_{sr}}|}\right) \tag{1}$$

To find the surface local azimuth ϕ_s, first the surface local x-axis needs to be defined. As mentioned in section II-A, this axis should lie within the global xz-plane. This combined with the fact that the surface local angle should be orthogonal to the surface normal vector, results in (2).

$$\hat{x}_s = \frac{\hat{y} \times \hat{n}_s}{|\hat{y} \times \hat{n}_s|} \tag{2}$$

The last remaining surface local axis, $\hat{y}_s$ can simply be found by computing $\hat{n_s} \times \hat{x_s}$.

The surface local azimuth can subsequently be found by transforming $\vec{r_{sr}}$ to the surface local system and then taking the arctangent of the x- and y-components, resulting in (3).

$$\phi_s = \tan^{-1}\left(\frac{\hat{y}_s \cdot \vec{r_{sr}}}{\hat{x}_s \cdot \vec{r_{sr}}}\right) \tag{3}$$

The radial velocity $\vec{v_r}$ can be found by computing the projection of the velocity of the car in the direction of $\vec{r_{sr}}$ as shown in (4).

$$v_r = \frac{\vec{r_{sr}} \cdot \vec{v_c}}{|\vec{r_{sr}}|} \tag{4}$$

As $\vec{r_{sr}}$ is the vector from the surface point to the radar, the radial velocity for objects moving towards the radar is negative, while the radial velocity for objects moving away is positive.

The radar local observation angles θ_r and ϕ_r can be found by first transforming $\vec{r_{sr}}$ to the radar local coordinate system and subsequently using a transformation to spherical coordinates. This transformation can be performed using (5).

$$\vec{r_{sr,r}} = \begin{bmatrix} 1 & 0 & 0 \\ 0 & \cos(\pi - \alpha) & -\sin(\pi - \alpha) \\ 0 & \sin(\pi - \alpha) & \cos(\pi - \alpha) \end{bmatrix} (\vec{p_s} - \vec{p_r}) \tag{5}$$

Transformation to spherical coordinates subsequently results in $\theta_r = \cos^{-1}\left(\frac{\vec{r_{sr,r}}}{|\vec{r_{sr,r}}|}\right)$ and $\phi_r = \tan^{-1}\left(\frac{\vec{r_{sr,r}} \cdot \hat{y}}{\vec{r_{sr,r}} \cdot \hat{x}}\right)$.

III. Application to Rough Surface without Undulations

Using the equations derived in section II-B, the signature for a rough surface without undulations, i.e. a flat, straight surface, is computed. In this specific case, the surface z-coordinate for all surface points is 0 and the normal vector of this surface is equal to $\hat{z}$ everywhere. This also implies that the surface local system has the same orientation as the global system. Furthermore, it is assumed that the scattering from the road surface is isotropic, meaning that the radar cross-section (RCS) of a surface point is no longer a function of ϕ_s.

First, the θ_s^{flat} angle for the rough surface without undulations is derived. This is determined to be

$$\theta_s^{flat}(x, y) = \cos^{-1}\left(\frac{h_r}{\sqrt{x^2 + y^2 + h_r^2}}\right). \tag{6}$$

The radial velocity v_r^{flat} for this surface is found to be

$$v_r^{flat} = \frac{v_c y}{\sqrt{x^2 + y^2 + h_r^2}}. \tag{7}$$

The expressions for the local radar observation angles are a bit more intricate. The θ_r^{flat} angle can be computed using

$$\theta_r^{flat} = \cos^{-1}\left(\frac{y \sin(\pi - \alpha) - h_r \cos(\pi - \alpha)}{\sqrt{x^2 + y^2 + h_r^2}}\right). \tag{8}$$

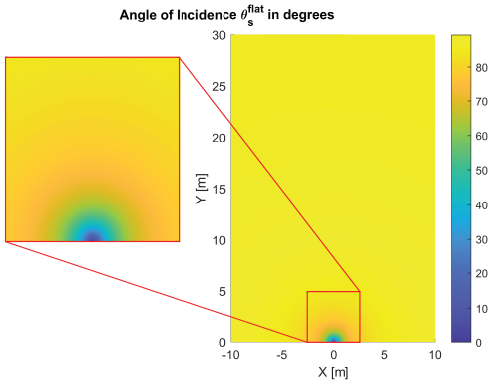

Fig. 2. Angle of incidence θ_s^{flat} for a surface without undulations for a radar mounting height h_r of 50 cm.

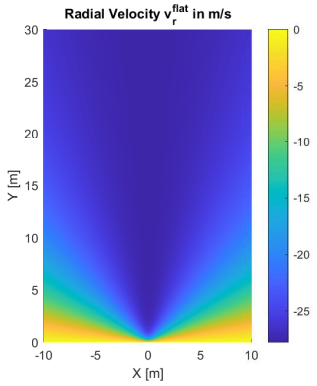

Fig. 3. Radial velocity v_r^{flat} for a surface without undulations with a radar mounting height h_r of 50 cm and a platform velocity v_c of 100 km/h.

Similarly, ϕ_r^{flat} can be calculated using

$$\phi_r^{flat} = \tan^{-1}\left(\frac{y\cos(\pi-\alpha)+h_r\sin(\pi-\alpha)}{x}\right). \quad (9)$$

Using the derived expressions, the variation in radial velocity and incident angles over a rough surface without undulations can be studied. Fig. 2 shows θ_s^{flat} as function of x and y for such a surface. This figure shows that θ_s^{flat} varies strongly close to the car due to the mounting height of the radar, but this variation reduces quickly. When this angle is compared at 5 m and 6 m respectively, the difference between these ranges has dropped to below 1 degree. Depending on the scattering characteristics of the observed surface, the RCS of one range bin can be simulated by plane wave incidence.

Besides this, Fig. 2 can also be used to evaluate the change in incident angle over the coherent processing interval of the radar system. Assuming a coherent processing interval of 1 ms, an observed surface point will experience a range migration of 42 mm when the car is moving with a velocity of 150 km/h. This shows that the change in angle of incidence, and by extension the scattering characteristics, will not vary significantly over the coherent processing interval.

Fig. 3 shows the radial velocity of each point on the surface without undulations. It can be seen that the radial velocity over the surface does not vary significantly directly in front of the vehicle, but shows stronger variation directly to the left and the right of the car. This causes the road surface to have different radial velocities smearing its signature in a range bin over the Doppler domain. The severity of this effect depends on the cross-range resolution of the radar and on the car's velocity.

IV. Range-Doppler Signature of a Flat Asphalt Surface

Using the results obtained from sections II and III plus information on the radiation pattern of the radar and the RCS σ_s of a surface patch, the range-Doppler signature can be derived. Regarding the radiation pattern of the radar, in this example a simple $\cos\left(\theta_r^{flat}\right)$ pattern is assumed.

Furthermore, a realistic asphalt road surface is considered in this example. To determine if the roughness of asphalt is significant at mm-wave frequencies, which is important for considering the RCS, the statistical properties of the sample were determined. The surface profile of this sample was digitised by means of a CT-scan, courtesy of the Pavement Lab of the CITG faculty of TU Delft. From this digitised surface shown in Fig. 4, it is determined that the RMS height of this scanned sample is 2.1 mm and its correlation length 2.2 mm. At a frequency of 79 GHz, these statistical properties are more than half a wavelength and thus surface roughness should be taken in account.

As the surface profile of asphalt is geometrically complex, a numerical approach is taken to determine its RCS as a function of incident angle and frequency. The asphalt surface geometry differs from patch to patch, and so the RCS may differ from patch to patch. Therefore, the statistical properties of the RCS should be determined. In order to do this, a Monte-Carlo approach is taken. In this method, the RCS of many surface samples is determined to find the statistical properties.

However, the digitisation of asphalt surface profiles using CT-scans is a complex and expensive process, unfeasible for all possible surfaces, and thus an alternative way to obtain realisations of asphalt road surface samples needed to be found. The method that was devised is to generate synthetic asphalt surface samples based on the digitised surface that was obtained by CT-scan.

The synthetic surface generation starts by obtaining the cumulative distribution function of the scanned surface sample and computing its spatial spectrum by applying a Fourier transform. Subsequently, a surface is generated by appointing each x, y grid point a height generated following an uniform distribution. Next, the generated surface is transformed to the spectral domain and is filtered such that its amplitude spectrum has approximately the same shape as that of the scanned sample. Finally, a probability integral transform and an inverse probability integral transform are performed to ensure similarity of the cumulative distribution functions of the scanned and generated sample. It should be noted that this algorithm is able to generate synthetic surfaces of arbitrary size.

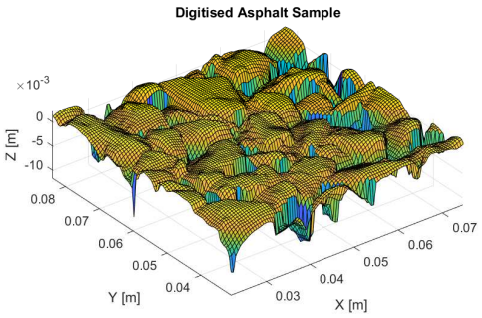

Fig. 4. Digitised asphalt road surface sample.

Numerical simulations to determine the statistics on the RCS of asphalt road surfaces are currently ongoing. In order to already obtain a range-Doppler signature, in this example the RCS of an asphalt surface patch is assumed to be independent of angle of incidence and frequency. Hence, the RCS of each surface patch in this scenario is the same. To generate the range-Doppler map, the received power for each surface patch is calculated and then summed to the corresponding range-Doppler bin. This received power is calculated using the radar equation. This results in the range-Doppler map shown in Fig. 5 (left). This figure clearly shows the spreading of the road surface signature over the Doppler domain. Furthermore, it can be seen that the radar radiation pattern reduces the power received from cells that present low Doppler-shifts as these cells are orthogonal to the direction of travel of the car. Lastly, it can be seen that most of the backscattered signal is concentrated in close range bins due to the fourth power range dependence, and that more power is received from patches with high Doppler-shift compared to those with low Doppler-shift.

Fig. 5 (right) shows also a range-Doppler map of an automotive radar measurement performed whilst driving at about 15 km/h on a public road. Here, the road surface signature can clearly be recognised, matching in shape with the proposed model (red dashed line). The measured range-Doppler map contains another extended target at further range which corresponds to a building on the side of the road. In this measurement, the radar was mounted on the front bumper of a car at a height of approximately 40 cm and with an angle α of 90 degrees. The radiation pattern of the radar in this measurement can be approximated by a $\cos\theta$ shape.

V. Conclusion

This paper has presented a method to compute the dynamic signature of road surfaces in automotive scenarios. This has been applied to a flat asphalt rough surface taken from a realistic road sample. For the first time in literature, road surface scattering has been analysed as a dynamic process and presented in the form of a range-Doppler plot. This result has been compared to an automotive radar measurement performed whilst driving on a public road and good agreement between model and measurement has been demonstrated. It has been shown for the first time in literature that the geometrical effects of the automotive scenario cause the road surface signature to spread over Doppler.

Besides this, it has been concluded that over a coherent processing interval the Doppler-shift does not change significantly for an observed range cell. Similarly, the change in incident angle over a range cell has been shown to be small. However, depending on the scattering characteristics of the surface, this may be significant and needs to be taken into account for computation of backscattering from the road.

The results of this study can build up to later research to classify road surfaces and identify road hazards such as puddles of water or patches of ice using automotive radar. This could in turn lead to an enhancement of road safety. For example, this work can be used to isolate the contribution from road surface scattering from the range-Doppler plot and perform a statistical analysis only on the relevant cells. Also, the model presented in this work could be used in the future to determine the most distinguishing features of different surface scattering contributions for use in classification algorithms.

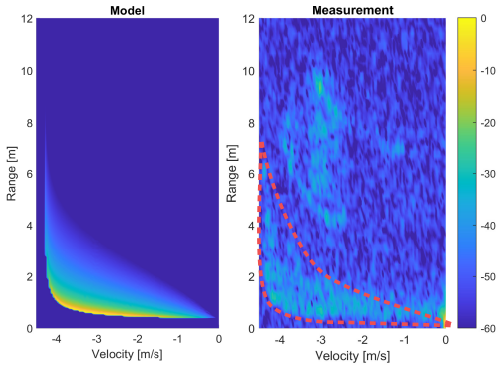

Fig. 5. Comparison of predicted (left) and measured (right) normalised range-Doppler signatures in decibels of an asphalt road surface when the car is moving at a speed v_c of 15 km/h.

Acknowledgment

The authors are grateful to Dr. K. Varveri for providing the digitised CT-scan of an asphalt road surface sample.

References

[1] J. Hasch, E. Topak, R. Schnabel, T. Zwick, R. Weigel, and C. Waldschmidt, "Millimeter-Wave Technology for Automotive Radar Sensors in the 77 GHz Frequency Band," *IEEE Trans. Microw. Theory Techn.*, vol. 60, no. 3, pp. 845–860, 2012.

[2] K. Sarabandi, E. S. Li, and A. Nashashibi, "Modeling and Measurements of Scattering from Road Surfaces at Millimeter-Wave Frequencies," *IEEE Trans. Antennas Propag.*, vol. 45, no. 11, pp. 1679–1688, 1997.

[3] E. S. Li and K. Sarabandi, "Low grazing incidence millimeter-wave scattering models and measurements for various road surfaces," *IEEE Trans. Antennas Propag.*, vol. 47, no. 5, pp. 851–861, 1999.

[4] A. Bystrov, E. Hoare, T. Y. Tran, N. Clarke, M. Gashinova, and M. Cherniakov, "Automotive system for remote surface classification," *Sensors (Switzerland)*, 2017.

[5] P. Asuzu and C. Thompson, "Road condition identification from millimeter-wave radar backscatter measurements," in *2018 IEEE Radar Conference (RadarConf18)*, 2018, pp. 0012–0016.